Bull Earthquake Eng (2015) 13:83–95
DOI 10.1007/s10518-014-9607-z

ORIGINAL RESEARCH PAPER

Nonlinear analysis of earthquake fault rupture interaction with historic masonry buildings

Marianna Loli · Ioannis Anastasopoulos · George Gazetas

Received: 17 June 2013 / Accepted: 9 March 2014 / Published online: 25 March 2014

Abstract The response of historic masonry buildings to tectonic ground displacements is studied through analysis of a simple yet representative soil–foundation–masonry wall system. A nonlinear 3D finite element method is developed and employed to reproduce the strong nonlinear response of the rupturing soil, as well as the masonry structure. Following a sensitivity analysis of the effect of the exact location of the structure with respect to the emerging fault, the paper discusses several characteristic mechanisms of soil–structure interaction and evaluates the associated structural distress. The observed failure pattern and the consequent structural damage are shown to depend strongly, varying from minimal to dramatic, on the exact position of the structure relative to the fault. Alleviation of tectonic risk through foundation enhancement/improvement is investigated by considering alternative foundation systems. Results highlight the advantageous performance of rigid embedded and continuous foundations as opposed to more flexible and isolated supports indicating that foundation strengthening may provide important shielding against settlement and structural drift.

Keywords Masonry structure · Tectonic faults · Monument · Nonlinear analysis · Mitigation measures

1 Introduction to the studied problem

Besides being the generation source of earthquakes sending off waves in the surrounding medium, tectonic faults may also directly affect above-ground structures by means of permanent ground displacements. This is likely to be the case in large magnitude and/or shallow earthquakes, when the causative fault propagates all the way to the ground surface, causing permanent ground deformation thereby imposing significant distress to overlying structures. A significant number of case studies may be found in the literature documenting a variety of

M. Loli · I. Anastasopoulos (✉) · G. Gazetas
National Technical University, Athens, Greece
e-mail: i.anastasopoulos@dundee.ac.uk

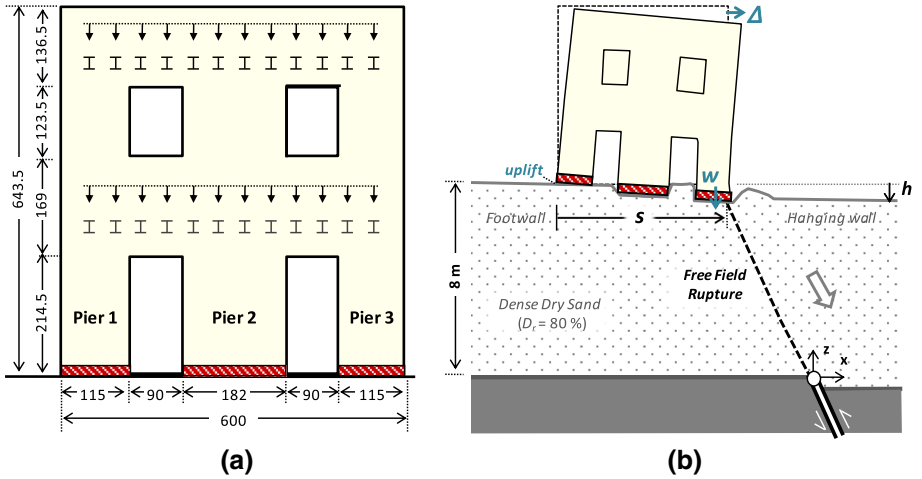

Fig. 1 Definition of the problem: **a** geometry of the masonry wall as adopted by Magenes et al. (1995) (with dimensions shown in centimetres); **b** Schematic of fault–soil–structure interaction mechanism and key parameters

structural failures due to interaction with the surface fault rupture in various large magnitude earthquakes around the globe (e.g. Chang et al. 2000; Kelson et al. 2001; Kawashima 2001; Angelier et al. 2003; Bray and Kelson 2006; Anastasopoulos and Gazetas 2007a,b; Faccioli et al. 2008).

Although the response of historic structures subjected to tectonic loads has not been explicitly addressed in the literature, it is evident that, given their significantly longer lifetime expectancy and in many cases their relatively large size, monuments are more likely than most other structures to experience such a tectonic hazard. Moreover, even if modern structures could be designed to withstand or relocated to avoid active faults that are already known, this is presumably inapplicable to monuments. Hence, it is necessary to account for faulting-induced loading in the seismic assessment and retrofit of historic structures in seismically active areas.

Being part of a major European project which dealt with the seismic protection of monuments in the Mediterranean [Lagomarsino et al., 2010], this paper presents research findings on the analysis, assessment and mitigation of tectonic risk for historic masonry structures. To this end, a rather rudimentary yet quite illustrative single-wall structure is selected for analysis. Depicted in Fig. 1a, its geometry is that of the well documented "door-wall" used in the large scale experiments of Magenes et al. (1995). Having a total height of 6.4 m and a thickness of 0.25 cm, the wall carries the dead weight of two floors ($N_{F1} = 248$ kN and $N_{F2} = 237$ kN) through three shear walls (Piers 1–3). In agreement also with the physical model studied by Magenes and his co-workers, the structure is made of unreinforced masonry, consisting of solid fired-clay bricks and mixed hydraulic mortar, representing typical old urban construction in many European cities.

The masonry structure is founded on an 8 m thick layer of dense dry sand which is subjected to normal tectonic dislocation of vertical offset h at the underlying bedrock (Fig. 1b) with a dipping angle of 60°. As a result, the hanging wall (displaced block) moves downwards following the fault dip and if the structure did not exist (i.e., in free field conditions), the fault deformation would localize on a rupture plane as indicated by the dashed line. The presence of the structure modifies the rupture pattern, and the foundation–

structure system experiences some permanent displacement. For the sake of brevity, the performance of the structure will be assessed on the basis of the roof drift Δ and the foundation settlement w.

Preliminary numerical analyses (Loli et al. 2012b) have indicated that the exact response of the system depends profoundly on the exact position of the structure with respect to the emerging fault. The location is quantified with the distance s, measured from the left (footwall side) corner of the structure to the point where the free field rupture plane would have emerged without the presence of a structure. This distance is normalized by the total width of the structure, $B = 6$ m.

The structure is first considered standing on isolated footings—the benchmark case. In a subsequent step, the effect of foundation type is addressed. Comparison of the benchmark case response with the response of the same structure supported on a flexible strip foundation, as well as on isolated or continuous embedded foundations, illustrates the role of foundation type in the prevailing mechanisms of fault–structure interaction and the overall system performance. Accompanied with a parametric study on the sensitivity to the exact location of the structure, the analysis aims at: (1) achieving a comprehensive assessment of tectonic risk to such masonry structures, representative of historic buildings around the Mediterranean and elsewhere, and (2) showing the potential to mitigate this risk through foundation enhancement.

2 Numerical methodology

Former studies have shown that the finite element (FE) method can simulate the phenomenon of fault rupture propagation in the free field with reasonable accuracy (e.g. Bray et al. 1994; Anastasopoulos et al. 2007; Loukidis et al. 2009), as well as its interaction with surface foundations (Anastasopoulos and Gazetas 2007b; Anastasopoulos et al. 2009) and rigid embedded foundations (Loli et al. 2012a). In view of the importance of footing shape effects, 3D FE is employed (using ABAQUS) to realistically simulate the studied problem.

Figure 2a shows a typical deformed FE mesh and highlights modelling details and boundary conditions for the benchmark problem (i.e., wall on isolated footings). Three additional models are built with the only variation being in the type and geometry of the foundation. More specifically, three foundation alternatives were considered: a shallow (continuous) strip foundation; embedded spread footings (at depth $d = 0.5$ m); and an embedded (continuous) strip foundation of the same embedment depth. The respective deformed FE meshes are portrayed in Fig. 2b.

The soil is discretized into nonlinear 8-noded continuum elements, the response of which is governed by the elasto-plastic constitutive model described by Anastasopoulos et al. (2007). It defines failure using the Mohr–Coulomb failure criterion and employs isotropic strain softening to degrade the friction (φ) and dilation (ψ) angles linearly with plastic strain so as to reproduce the faulting associated mechanisms of shear localization and propagation of rupture planes.

This well-established constitutive relationship, which has been thoroughly validated against a number of experimental studies (Bransby et al. 2008a,b; Loli et al. 2011, 2012a) and shown to satisfactorily reproduce the strong nonlinear response of cohesionless soil materials under such excessive shear deformation, is herein extrapolated to model the nonlinear masonry material behaviour as well. Hence, yielding of the masonry material is defined by the Mohr–Coulomb criterion and, and similarly to the soil material, linear degradation

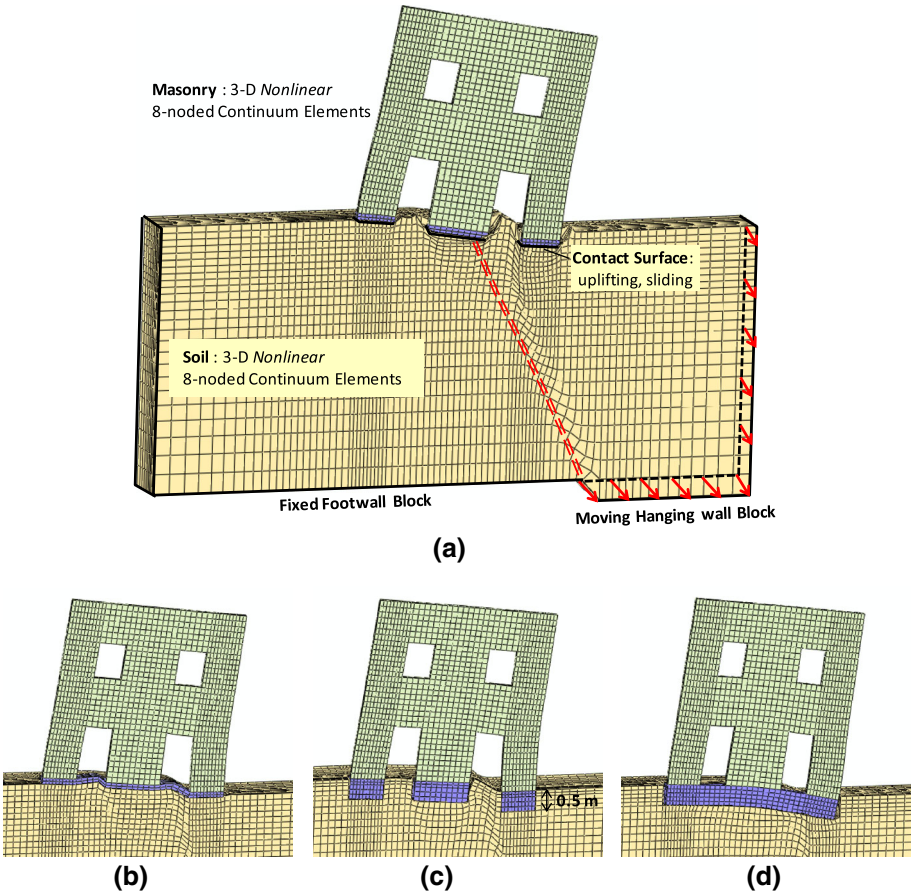

Fig. 2 Numerical modelling details. **a** Deformed FE mesh for the benchmark case wherein the wall is supported on isolated footings; and the three foundation alternatives: **b** raft foundation; **c** embedded foundation; and **d** continuous box-type foundation

of strength is assumed to take place with increasing octahedral plastic strain (γ_{oct}^{pl}) until a critical friction angle is reached, according to the following relationships:

$$\varphi;\psi = \begin{cases} \varphi_p - \frac{\varphi_p - \varphi_{cs}}{\gamma_f^{pl}}\gamma_{oct}^{pl};\ \psi_p\left(1 - \frac{\gamma_{oct}^{pl}}{\gamma_f^{pl}}\right), & for \quad 0 \le \gamma_{oct}^{pl} < \gamma_f^{pl} \\ \varphi_{cs};\ 0, & for \quad \gamma_{oct}^{pl} \ge \gamma_f^{pl} \end{cases} \tag{1}$$

where, φ_p and ψ_p the peak mobilized friction and dilation angles; φ_{cs} and ψ_{cs} their residual values; and γ_f^{pl} the octahedral plastic shear strain at the end of softening. Similarly, a linear softening relationship was attributed to the cohesion c of the masonry material, while the pre-yielding behavior is assumed to be elastic, characterized by the secant Young's modulus E.

While this assumption may be a crude reproduction of a much more complex reality, unavoidably ignoring the anisotropy and inhomogeneity of the masonry material, it was accepted as a reasonable compromise for the sake of permitting a comprehensive numerical

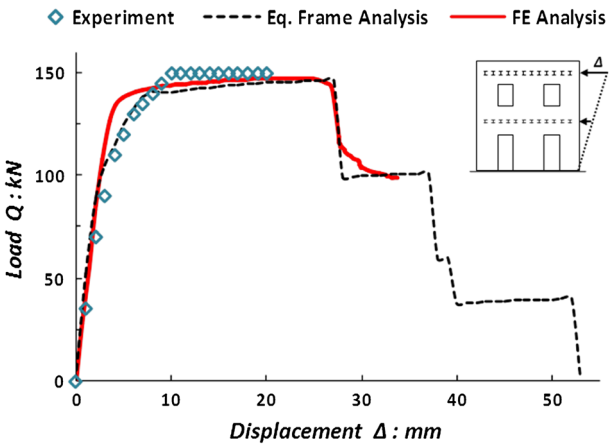

Fig. 3 Calibration of nonlinear masonry material model with reference to pushover test results (Magenes et al. 1995) and comprehensive macroelement analysis using the equivalent frame method (Galasco et al. 2004)

Table 1 Material modelling details

Parameter	Soil	Masonry
Young's modoulus [E (MPa)]	$0.5\,\sigma_V + 6$	1,500
Poisson's ratio	0.3	0.2
Peak friction angle [ϕ_p (deg)]	40	48
Critical friction angle [ϕ_{CS} (deg)]	32	34
Peak dilation angle [ψ_p (deg)]	10	18
Critical dilation angle [ψ_{CS} (deg)]	2	4
Peak cohesion [c_p (kPa)]	–	200
Critical cohesion [(c_{CS} (kPa)]	–	2

study of the entire soil–foundation–structure system interacting with a rupturing fault. This is an extension to a previous study in which a hybrid 2-step analysis methodology was presented (Loli et al. 2012a,b). In the first step, fault rupture–soil–structure interaction was modelled with FE assuming elastic masonry response. In the second step, the computed foundation deformation was used as the input to compute structural distress of the masonry wall, using a sophisticated macroelement model (Galasco et al. 2009). However, the deformation of the foundation is strongly affected by the nonlinearity of the structure, and hence a 1-step analysis procedure is considered more realistic, despite the aforementioned limitations.

Constitutive relationships for the specific masonry material were calibrated with respect to the results of the real scale pushover tests performed at the University of Pavia by Magenes et al. (1995). Figure 3 demonstrates the quite satisfactory agreement achieved between experimental and numerical results in terms of the lateral load–displacement pushover response. Although it somewhat overestimates the post yielding stiffness of the system, the model predicts well the maximum lateral capacity of the wall. Moreover, compared to the results of a sophisticated macroelement analysis implemented within the Tremuri software (Galasco et al. 2009), the model also appears to capture the ductility capacity of the wall and the abrupt strength degradation associated with ductility exhaustion and collapse. Table 1 sums up the constitutive model parameters used for both soil and masonry materials.

In addition to inelasticity, the response is dominated to a large extent by second order (geometric) nonlinearities taking place at the soil–foundation interface. In many cases, downward movement of the hanging wall, causing settlement of the foundation on the hanging wall side, may be accompanied by significant uplift of the opposite (footwall) side, as well as foundation sliding along the interface, aggravating structural distress. Hence, it is considered essential to realistically simulate interface behaviour. Contact elements are utilized to this end, allowing detachment (loss of contact at zero pressure) and sliding (with friction coefficient $\mu = 0.5$ between masonry and soil).

3 Characteristic results

Due to length limitations, a comprehensive presentation of all the results is not possible; instead, an overview of the structural performance is attempted, focussing mainly on the magnitude of faulting-induced structural displacements.

Figure 4 illustrates the dominating effect of the exact foundation position on the displacements imposed on the structure after its interaction with the normal fault rupture. The roof drift Δ (Fig. 4a) and the foundation vertical movement w (Fig. 4b), which can be either negative or positive indicating settlement or uplift respectively, are measured at the footwall side corner, at the centre, and at the hanging wall side corner. These are plotted with respect to the normalized position parameter s/B for 0.6 m of bedrock dislocation. A remarkable

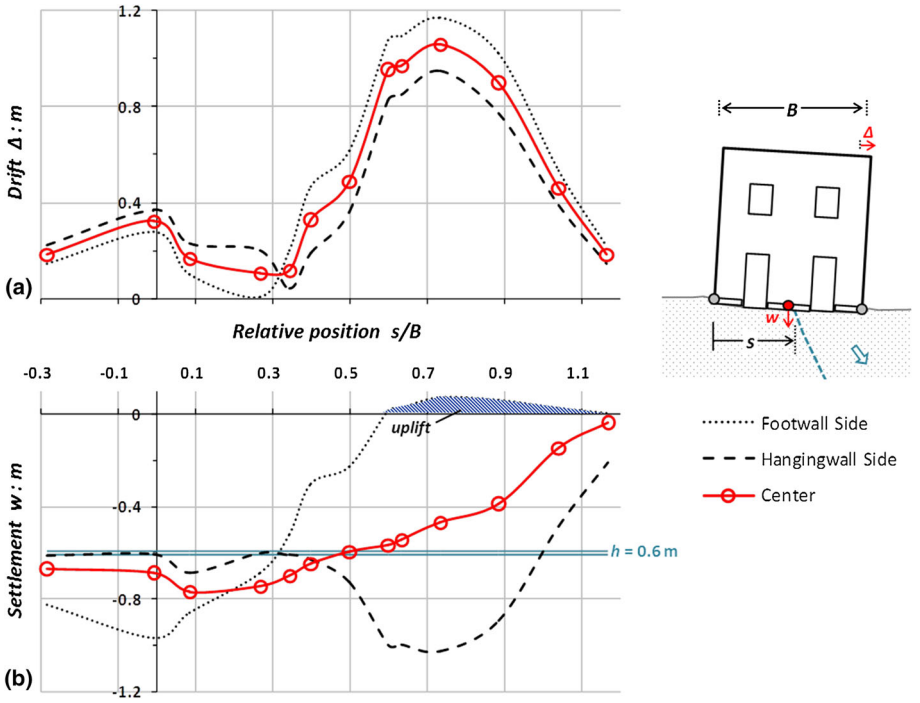

Fig. 4 Structural displacement with respect to the normalized position parameter (s/B) in terms of: **a** floor drift Δ and **b** foundation settlement w at the two edges (footwall side and hanging wall side) of the structure and its centre point for 0.6 m of fault offset

variation in the magnitude of structural displacements may be readily observed even for small changes in the location of the fault relative to the structure. It is interesting to note that a shift of about 1 m (namely $s/B \approx 1/5$) in the location of the structure may result in more than double drift Δ.

The mechanisms lying behind this key role of parameter s are elucidated in Fig. 5, which portrays a set of four cross-sectional views of the deformed FE mesh with superimposed plastic strain contours for four different locations of the masonry wall. Plastic strain localizations indicate in each case the prevailing soil failure mechanism, characterized mainly by the propagation of fault deformation, but also by the additional soil deformation due to changing distribution of structural loads. The accompanying plots of vertical displacements δ_z along the soil surface and the foundation level indicate the effect of the presence of the structure on the ground deformation profile (in comparison with the free field case).

The following points are worthy of note:

(a) $s/B = 0$—In this case the free field fault (shown with the black dashed line) marginally interacts with the structure, outcropping just at its footwall side corner. Evidently, the presence of the structure at this position, has a very limited effect on the deformation profile of the ground surface in comparison to the free field response (Fig. 5a). Yet, some considerable exaggeration of the surface scarp height (emerging by the footwall corner of the structure) may be observed, presumably due to the excess shearing and failure of the soil supporting Pier 1. As a result, Footing 1 (supporting Pier 1) settles markedly more than the other two which, following the downward movement of the hanging wall, experience vertical displacements almost equal to the fault offset h. As a consequence, we notice the counter-clockwise rotation of the whole structure, despite its location on the downward moving block. Similar is the case, as is evident in Fig. 4b, for the range of possible locations $-0.3\text{B} < s < 0.3\text{B}$, or in other words when the fault crosses the foundation level at the footwall side of the central pier, or further towards the footwall. Here, structural distress is in general characterized by settlement of all three footings of the order of h (or more for the footwall side) but relatively low drift levels (Fig. 4a) as the entire structure practically follows the translational (downward) movement of the hanging wall.

(b) $s/B = 0.5$—When the free field rupture outcrops just underneath the midpoint of the foundation level, which is the centre of the footing supporting Pier 2, soil deformation spreads within a quite wide area spanning the entire structural width and causing diffusion of soil deformation (Fig. 5b). A shear localization plane may still be identified, having the same dipping angle with the free field rupture up to the middle of the soil stratum but deviating towards the hanging wall as it propagates further up to the surface, forming a steeper rupture as to avoid the "burden" of Footing 2; it eventually outcrops at the right side door opening. Yet, there appears to be no formation of a distinct scarp, as is the case in the free field. Instead, surface deformation concentrates on the soil bulges formed at the two door openings as a gradual clockwise rotation of the foundation level takes place. In contrast to what was the case in the previously described position, here the footwall corner settles significantly less than the two other footings (Fig. 4b), while structural drift is only marginally increased (Fig. 4a).

(c) $s/B = 0.73$—Fig. 5c indicates how the fault–soil–structure response changes when the structure is hit by the emerging rupture just 1 m further away towards the hanging wall (with respect to the previous case). This is certainly the most detrimental position, at least as far as structural displacements are concerned. It should be noted that this position is a representative example of the fault–soil–structure interaction mechanisms taking

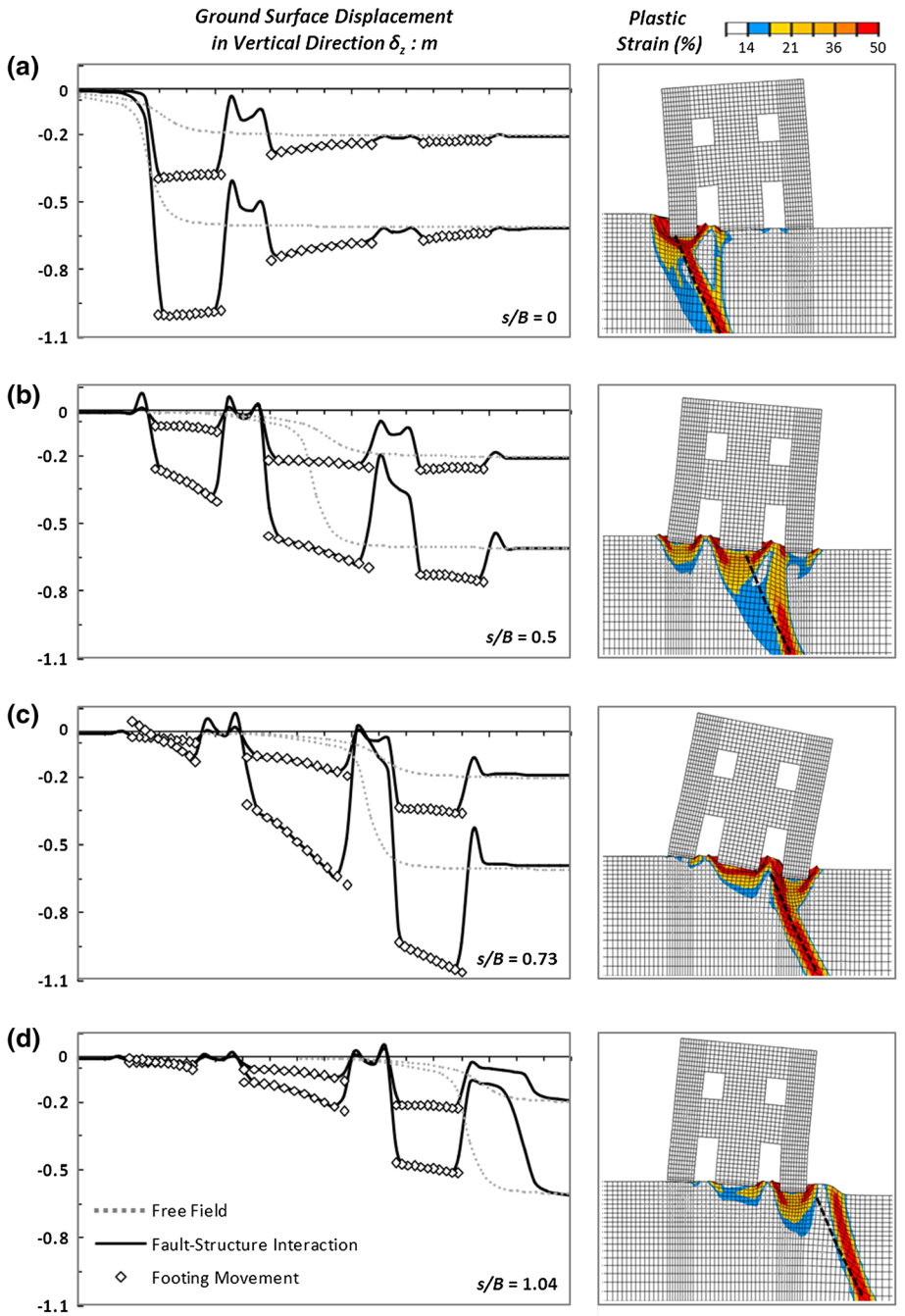

Fig. 5 Fault–soil–structure interaction mechanisms with respect to the normalized position parameter (s/B). Ground surface displacement profiles ($h = 0.2$ and 0.6 m) in comparison to free field conditions. The associated soil rupture patterns ($h = 0.6$ m) are indicated by deformed FE meshes with superimposed plastic strains for: **a** $s/B = 0$ m; **b** $s/B = 0.5$; **c** $s/B = 0.73$; and **d** $s/B = 1.04$

place at the whole range of positions from $s/B \approx 0.6$ to 0.9. Here, the propagating rupture intersects with the hanging wall corner of Footing 2. The deformed FE mesh snapshot shows that for 0.6 m of fault offset the primary rupture outcrops at the right door opening being slightly deviated towards the hanging wall (in comparison to free field). A secondary branch forms within the top 2 m (or so) of soil to intersect the hanging wall corner of Footing 3 and outcrop right beside it. As a result, these two rupture planes form a wedge around Footing 3 which dramatically increases its vertical displacement. Such a substantial settlement of the hanging wall corner makes the whole structure to rotate significantly, clockwise, as much as to lead to spectacular uplifting of the opposite (footwall side) corner. Vertical displacement profiles of Fig. 5c show that for $h = 0.6$ m almost half of the foundation area supporting Pier 1 looses contact with the ground. Naturally, such strong distress of the foundation results in drastic increase of the structural drift Δ. It should be noted that the entire range of structural positions $0.6 < s/B < 0.9$ is similarly characterized by peak drift response, almost double the amount experienced in other locations (Fig. 4a), and increased settlement of Footing 3 accompanied by uplifting of Footing 1 (Fig. 4b).

(d) $s/B = 1.04$—This is an interesting structural position, where the free field fault would be expected to emerge beyond the structure. If no interaction with the foundation–structure system were to take place, the structure would stand unscathed on the undisplaced footwall. Intuitively, one would anticipate this to be the least detrimental of the examined structural positions. Yet, as revealed by Fig. 4, this is not exactly the case. Quite surprisingly, in this position the masonry wall is subjected to similar or greater drift than for the range of positions $s/B < 0.5$, i.e. when the fault crosses the foundation level anywhere within its left (footwall side) half width. Moreover, although Footing 2 remains practically firm (almost unaffected), Footing 3 experiences considerable settlement while some uplifting of the footwall side corner of Footing 1 takes place. Figure 5d illustrates the relevant soil–structure interaction mechanisms. Namely, propagation and outcrop of the fault rupture in the vicinity of Footing 3 unavoidably causes its downwards movement and as a result formation of bearing capacity failure mechanisms underneath. Its differential settlement sheds load onto the other two foundations and naturally brings about some substantial clockwise rotation of the system.

4 Foundation role in the mitigation of tectonic risk

Seismic code provisions usually suggest that structures should be relocated to avoid seismically active tectonic faults. Limited as this practice may be, due to the fact that large magnitude earthquakes quite often occur upon historically unknown faults, it is moreover presumably inapplicable to the case of monuments. Hence the necessity for development of a valid methodology for the protection of historic buildings against tectonically induced permanent displacement load has motivated a number of studies (e.g., Bray 2001; Oettle and Bray 2013; Fadaee et al. 2013) investigating alternative mitigation measures. This paper deals with the potential of achieving this goal through foundation strengthening, motivated from the acknowledgment of the key role of the foundation in the prevailing mechanisms of fault–soil–structure interaction and the associated structural performance.

In view of the so far considered single wall masonry structure, the effect of the foundation type and characteristics in mitigating faulting-induced structural distress is assessed through comparison of the benchmark case (isolated footings) with the response of the

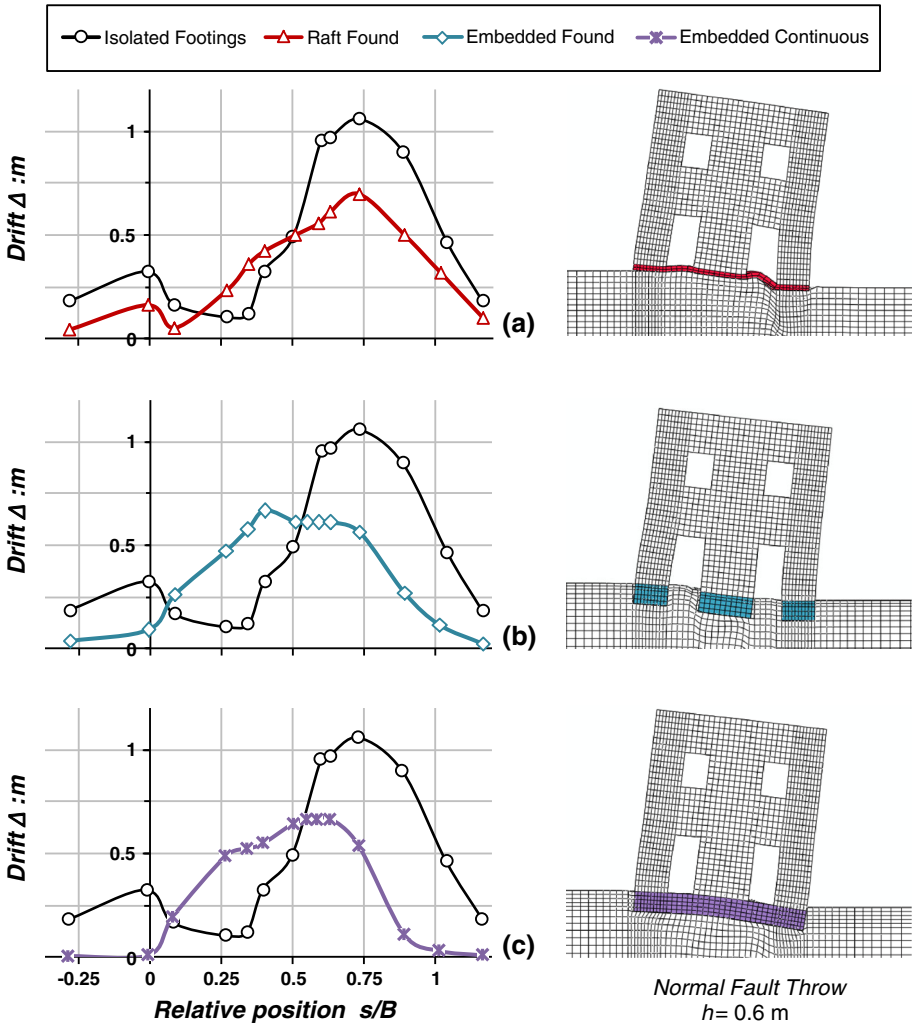

Fig. 6 Effect of the foundation type on the fault induced structural distress. Drift response envelopes, Δ, with respect to s/B, for $h = 0.6$ m in the three alternative foundation cases: **a** shallow strip; **b** embedded footings; and **c** continuous embedded strip foundation, all compared to the response of the wall on isolated footings

same structure on a number of foundation alternatives. Given the previously highlighted sensitivity to the exact position of the structure, such comparison is facilitated by considering response envelopes which encompass all the different mechanisms of response. Drift response envelopes ($\Delta - s/B$) are used in Fig. 6 to this end. The performance of the wall on isolated footings is compared to the response of three alternative (enhanced) foundation systems: a shallow continuous strip foundation (Fig. 6a); embedded isolated foundations with $d = 0.5$ m (Fig. 6b); and a continuous embedded strip foundation with $d = 0.5$ m (Fig. 6c). In all cases, the foundation is made by the same masonry material with the structure.

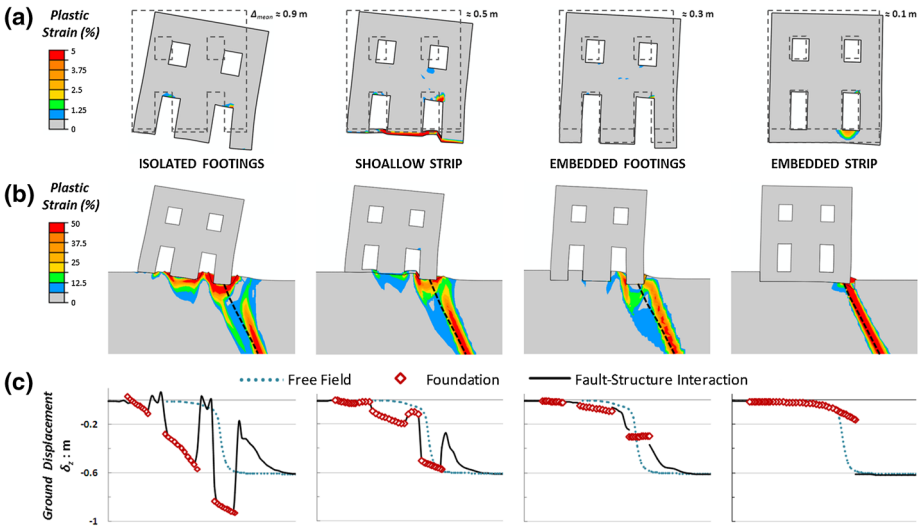

Fig. 7 Effect of the foundation type for $s/B = 0.88$: **a** deformed masonry wall and **b** deformed soil–structure system with superimposed plastic strains indicating shear localization mechanisms for $h = 0.6$ m; and **c** ground surface displacement profiles compared to free field response

Figure 6a indicates that foundation continuity may be quite beneficial in reducing structural drift displacements especially in the range of positions $0.5 < s/B < 1$ where peak response is observed. If standing on a shallow strip foundation the wall experiences generally lower drift amplitudes, reduced by a factor of 60% on average in the most detrimental location areas, in comparison to the benchmark case of isolated footings. Embedment appears to have an even stronger shielding effect, at least as far as the aforementioned most hazardous range of positions is concerned. When founded on embedded rather than shallow footings (Fig. 6b) the drift distress experienced by the wall is reduced to about the half in this area, or sometimes even more, if located elsewhere. Combining increased stiffness and continuity, the embedded strip foundation, certainly provides the most efficient means of mitigating structural drift distress. As shown in Fig. 6c, not only is the peak response plateau ($0.5 < s/B < 0.75$) reduced in height, but most importantly, the continuous embedded strip foundation diminishes structural distress in the areas $s/B > 1$ and $s/B < 0$ (this is when the fault outcrops outside the width of the foundation either towards the hanging wall or towards the footwall) hence "narrowing" the width of possible hazardous structural locations.

Despite the generally improved performance of systems standing on continuous and/or embedded foundations in comparison to isolated footings, it is important to observe that this effect is not totally consistent. Interestingly, there is a range of locations, namely for s/B between 0.25 and 0.5, or in other words when the free field rupture crosses the foundation level between the middle of the left (footwall side) door opening and the centre of the middle pier, where the benchmark structure experiences the lowest drift of all the studied systems. Yet, this is not an absolute advantage as in these locations the structure on isolated footings is subjected to significantly larger settlements.

Figure 7 summarizes the response of the four alternative wall–foundation systems for $s/B = 0.88$, where the beneficial effect of foundation embedment and continuity is quite significant. In this case the free field rupture path would cross the structure near its hang-

ing wall corner. As shown by the respective strain contours in Fig. 7b, shearing of the soil progressively becomes less widespread as foundation robustness increases through continuity and/or embedment. With one of its three supports (namely Footing 3) being subject to 0.6 m of tectonic dislocation, the very flexible foundation system with isolated footings is unable to withstand rotational movement towards the hanging wall, so much as to experience considerable uplifting on the opposite footwall side. Taking over increased axial loads Footings 2 and 3 result in experiencing excess settlements and the entire structure drifting abundantly towards the hanging wall. Thanks to its continuity, the strip foundation experiences significantly lower settlements under Piers 2 and 3 leading to quite reduced drift levels. Remarkable is the beneficial effect of foundation embedment in the other two cases and especially in the case of the continuous foundation. Owing to its significantly greater rigidity, the embedded strip foundation remains practically unaffected by the complete loss of support under its hanging wall corner resulting in minimal structural drift. Yet, as a drawback to the generally advantageous performance of continuous foundations, one should note that they are subjected to some considerable bending distress (see strain localizations in Fig. 7a).

5 Conclusions and limitations

The paper has dealt with the evaluation and mitigation of tectonic risk to historic masonry buildings in view of soil–foundation–structure interaction. A simplified numerical methodology was developed and employed in the 3D FE modelling of normal fault rupture interaction with a single wall masonry structure to simulate the strong nonlinear response of the rupturing soil and also capture the failure of masonry. An extensive parametric investigation was carried out demonstrating the great sensitivity of response to the exact location of the structure. Different interaction mechanisms dominate the response at different positions (this sensitivity being so pronounced as to significantly vary even for just 1 m shift in the structural location) and the associated structural distress may vary from minimal to dramatic. The analysis is focused on the effect of the foundation type and characteristics on the performance of the structure. Various alternative foundations were considered and their effectiveness in alleviating tectonically induced distress was assessed. Results highlight the significant advantage of foundation continuity and embedment in reducing permanent displacements imposed onto the structure suggesting that foundation enforcement may be a valid measure for the protection of historic buildings against tectonic risks.

It is important to highlight the main limitation of the presented numerical study, which refers to the simplified simulation of the nonlinear response of the superstructure. The employed constitutive relations cannot accurately capture the complex behaviour of masonry, as the nonlinearities which are associated with its anisotropy and inhomogeneity are not addressed. As a result, the model may be over-predicting the displacement capacity of the wall, and the excessively large values of permanent drift may not be realistic: in reality, the wall would probably collapse at such levels of deformation. It is believed that this limitation may affect the results in quantitative terms, but the key results and qualitative conclusions remain valid.

Acknowledgments The results have been achieved in the project PERPETUATE (www.perpetuate.eu), funded by the European Commission in the Seventh Framework Programme (FP7/2007–2013), under Grant Agreement No. 244229.

References

Anastasopoulos I, Gazetas G (2007a) Foundation–structure systems over a rupturing normal fault: Part I. Observations after the Kocaeli 1999 earthquake. Bull Earthq Eng 5(3):253–275

Anastasopoulos I, Gazetas G (2007b) Behaviour of structure–foundation systems over a rupturing normal fault: Part II. Analysis of the Kocaeli case histories. Bull Earthq Eng 5(3):277–301

Anastasopoulos I, Gazetas G, Bransby MF, Davies MCR, El Nahas A (2007) Fault rupture propagation through sand: finite element analysis and validation through centrifuge experiments. J Geotech Geoenviron Eng ASCE 133(8):943–958

Anastasopoulos I, Gazetas G, Bransby MF, Davies MCR, El Nahas A (2009) Normal fault rupture interaction with strip foundations. J Geotech Geoenviron Eng ASCE 135(3):359–370

Angelier J, Lee J-C, Hu J-C, Chu H-T (2003) Three-dimensional deformation along the rupture trace of the September 21st, 1999, Taiwan earthquake: a case study in the Kuangfu school. J Struct Geol 25:351–370

Bransby MF, Davies MCR, El Nahas A, Nagaoka S (2008a) Centrifuge modelling of normal fault–foundation interaction. Bull Earthq Eng 6(4):585–605

Bransby MF, Davies MCR, El Nahas A, Nagaoka S (2008b) Centrifuge modelling of reverse fault–foundation interaction. Bull Earthq Eng 6(4):607–628

Bray JD (2001) Developing mitigation measures for the hazards associated with earthquake surface 11 fault rupture. A workshop on seismic fault-induced failures—possible remedies for damage 12 to urban facilities. Japan Society for the Promotion of Science, pp 55–79

Bray JD, Kelson KI (2006) Observations of surface fault rupture from the 1906 earthquake in the 23 context of current practice. Earthq Spectra 22:S69–S89 S2

Bray JD, Seed RB, Cluff LS, Seed HB (1994) Analysis of earthquake fault rupture propagation through cohesive soil. J Geotech Eng ASCE 120(3):562–580

Chang K-C, Chang D-W, Tsai M-H, Sung Y-C (2000) Seismic performance of highway bridges. Earthq Eng Eng Seismol 2(1):55–77

Faccioli E, Anastasopoulos I, Callerio A, Gazetas G (2008) Case histories of fault–foundation interaction. Bull Earthq Eng 6:557–583

Fadaee M, Anastasopoulos I, Gazetas G, Jafari MK, Kamalian M (2013) Soil bentonite wall protects foundation from thrust faulting: analyses and experiment. Earthq Eng Eng Vib 12(3):473–486

Galasco A, Lagomarsino S, Penna A, Resemini S (2004) Non-linear seismic analysis of masonry structures. In: Proceedings of 13th WCEE, Vancouver, paper no 843

Galasco A, Lagomarsino S, Penna A, Cattari S (2009) TREMURI program: seismic analyses of 3D masonry buildings. University of Genoa, Genoa

Kawashima K (2001) Damage of bridges resulting from fault rupture in the 1999 Kocaeli and Duzce, Turkey earthquakes and the 1999 Chi-Chi, Taiwan Earthquake. In: Workshop on seismic fault-induced failures—possible remedies for damage to urban facilities, University of Tokyo Press, pp 171–190

Kelson KI, Kang K-H, Page WD, Lee C-T, Cluff LS (2001) Representative styles of deformation along the Chelungpu fault from the 1999 Chi-Chi (Taiwan) earthquake: geomorphic characteristics and response of man-made structures. Bull Seismol Soc Am 91(5):930–952

Lagomarsino S, Modaressi H, Pitilakis K, Bosjlikov V, Calderini C, D'Ayala D, Benouar D, Cattari S (2010) PERPETUATE Project: the proposal of a performance-based approach to earthquake protection of cultural heritage. Adv Mater Res 133–134:1119–1124

Loli M, Anastasopoulos I, Bransby MF, Ahmed W, Gazetas G (2011) Caisson foundations subjected to reverse fault rupture: centrifuge testing and numerical analysis. J Geotech Geoenviron Eng ASCE 137(10):914–925

Loli M, Bransby MF, Anastasopoulos I, Gazetas G (2012a) Interaction of caisson foundations with a seismically rupturing normal fault: centrifuge testing versus numerical simulation. Geotechnique 62(1):29–43

Loli M, Anastasopoulos I, Gazetas G, Cattari S, Degli Abbati S, Lagomarsino S (2012b) Response of historic masonry structures to tectonic ground displacements. In: Proceedings of 15th world conference on earthquake engineering, 24–28 Sept 2012, Lisboa, Portugal

Loukidis D, Bouckovalas G, Papadimitriou AG (2009) Analysis of fault rupture propagation through uniform soil cover. Soil Dyn Earthq Eng 29(11–12):1389–1404

Magenes G, Kingsley GR, Calvi GM (1995) Seismic testing of a full-scale, two-story masonry building: test procedure and measured experimental response. Experimental and numerical investigation on a brick masonry building prototype. CNR-GNDT, pp 1–41

Oettle NK, Bray JD (2013) Geotechnical mitigation strategies for earthquake surface fault rupture. J Geotech Geoenviron Eng ASCE 139(11):1864–1874